Aqueous ammonia abatement on Pt- and Ru-modified TiO_2: selectivity effects of the metal nanoparticles deposition method

Maria Vittoria Dozzi[a,*], Sabrina Brocato[a], Gianluigi Marra[b], Gabriella Tozzola[b], Laura Meda[b], Elena Selli[a]

[a] *Dipartimento di Chimica, Università degli Studi di Milano, via Golgi 19, I-20133 Milano, Italy*

[b] *Dipartimento di Energia, Dipartimento di Chimica Fisica, Istituto ENI Donegani, via G. Fauser 4, I-28100 Novara, Italy*

A B S T R A C T

A series of TiO_2 – based photocatalysts obtained by deposition of Pt nanoparticles (NPs) has been tested in the photocatalytic decomposition of aqueous ammonia under UVA irradiation. Two main deposition routes were employed, *i.e.* (i) the deposition of surfactant-stabilized preformed metal NPs and (ii) a modified version of the well-known deposition-precipitation technique, employing urea as precipitating agent. The effects that the deposition route and the amount of deposited metal have on both ammonia conversion (X_{NH3}) and selectivity (S_Y) towards the different N-containing products (Y = N_2, NO_2^-, NO_3^-) have been investigated systematically, in relation to the morphological distribution of NPs on TiO_2, as evidenced by HR-TEM analysis. The combination of Pt (0.8 wt.%) with a relatively low amount of Ru NPs (0.1 wt.%) as co-catalysts, both deposited on TiO_2 under optimized conditions, results in an exceptional stabilization of nitrite ions ($S_{NO_2^-}$ ~ 70%), from which N_2, the most desired ammonia oxidation product, might subsequently be obtained catalytically.

Keywords: Photocatalysis; TiO_2; ammonia oxidation; selectivity; metal nanoparticles

* Corresponding author at: Dipartimento di Chimica, Università degli Studi di Milano, via Golgi 19, I-20133 Milano, Italy. Tel.: +39 02 503 14237; fax: +39 02 503 14260.

E-mail address: mariavittoria.dozzi@unimi.it

1. Introduction

The photocatalytic oxidation of ammonia into nontoxic N_2 represents an unconventional and effective way to detoxify wastewaters originated from livestock manure. In fact, high concentration of NH_3 in wastewaters may provoke a dangerous accumulation of nitrogen-containing nutrients in soil and groundwater, accompanied by harmful eutrophication phenomena [1,2].

Although many efforts have been made in the last decades at finding valuable alternative materials to be employed as photocatalysts [3,4], TiO_2 still represents the best performing semiconductor material to be used for this purpose. In fact, TiO_2, being largely available, cheap and, most importantly, (photo-)stable, exhibits a pretty unique combination of suitable physico-chemical properties [5]. However, the preparation of TiO_2-based photocatalytic materials able to promote the selective conversion of ammonia into innocuous N_2 is still challenging, ammonia being easily photocatalytically converted into other pollutant species, such as nitrite and nitrate anions, which may be even more noxious than NH_3 itself [6].

The use of TiO_2 – based photocatalysts obtained by deposition of metal nanoparticles (NPs) on the TiO_2 surface was found to be effective in ammonia degradation [7–9], metal NPs acting as efficient traps of electrons photoexcited in the semiconductor, thus ensuring a better separation of photoproduced charge carriers and consequent higher rate of hole-mediated oxidation reactions [10–12]. However, though exhibiting good performance in terms of ammonia conversion, some metal-modified TiO_2 photocatalysts were not efficient in producing mildly oxidized products, and in particular to the most desired product of

ammonia oxidation, *i.e.* totally innocuous N_2 [13]. In fact, the mechanism of NH_3 photo-decomposition may be affected by the type of metal on TiO_2, as well as by its loading [13]. At the same time the paths of ammonia photodecomposition were found to be controlled by other experimental features, *e.g*. the photo-reactor design, the composition and flow rate of gases bubbling into the reaction medium, the pH conditions and the TiO_2 crystal phase [14–18].

In the present work we focus on the effects that the chemical route employed to deposit Pt NPs on commercial TiO_2 has on the photo-degradation of aqueous NH_3. In particular, two main Pt NPs deposition routes were chosen, *i.e.* (i) the deposition of surfactant-stabilized preformed metal NPs and (ii) a modified version of the well-known deposition-precipitation technique, employing urea as precipitating agent [19,20]. The potential effects induced on ammonia photodegradation paths by TiO_2 surface modification with Pt NPs have been explored in relation to both dimension and surface distribution of metallic NPs, which were shown to specifically depend on the adopted deposition method.

The effects that the combination of Pt and Ru NPs deposition on TiO_2 surface have on the photodegradation of aqueous NH_3 have also been explored, with the aim of efficiently exploiting the specific properties of each metal co-catalyst. In fact, while the overall ammonia conversion increases when Pt NPs are used as co-catalysts [13], ruthenium, which is successfully used in many industrially relevant catalytic processes [21–24], has peculiar effects in improving the selective performance of titania-based photocatalysts [25–27].

2. Experimental

2.1. Chemicals and materials

Aqueous ammonia (100 ppm of nitrogen, *i.e. ca.* 7.1 mM in NH_3, pH *ca.* 10-10.5) was prepared from a 28–30 wt.% aqueous NH_3 stock solution. P25 TiO_2 (Evonik) was used both as received and after modification by deposition of different metal NPs. Chloroplatinic acid hydrate (~ 38% Pt) and $RuCl_3 \cdot 3H_2O$ (>99%), purchased from Sigma–Aldrich, were employed as metal NPs precursor. A Fluka certified Multianion Standard Solution was used for ion chromatographic calibration and analysis. Ultra-pure water (18.2 MΩ cm), supplied by a Millipore Direct-Q3 water purification system, was employed to prepare all solutions.

2.2. Photocatalysts preparation

Two series of Pt/TiO_2 photocatalysts were prepared starting from commercial P25 TiO_2 powders. In the first preparation method, pre-formed Pt NPs stabilized by n-dodecyl trimethyl ammonium chloride were deposited on TiO_2 from colloidal suspensions, as described in detail elsewhere [28–30]. Briefly, the proper amount of metal precursor was dissolved in an aqueous solution containing the surfactant (40:1 surfactant to metal molar ratio). A metal colloidal suspension was then obtained by adding a large excess of $NaBH_4$ as reducing agent. An aliquot of this colloidal suspension was then added, under vigorous stirring, to a previously sonicated water suspension containing the required amount of photocatalyst powder. The so obtained powder was recovered, washed and dried overnight in an oven at 70 °C. The nominal loadings of Pt NPs on TiO_2 varied within the 0.3-0.8 wt.% range. The so-prepared photocatalysts series was named “C series” and the samples

were labeled as P25/Pt(x)C, with x indicating the Pt nominal weight percent loading with respect to TiO_2.

Alternatively, a modified version of the well-known deposition–precipitation (DP) technique was employed to deposit Pt NPs on P25 TiO_2 [19,20]. In this case, the required amount of TiO_2 was added to an aqueous solution containing the metal precursor (metal content 0.1 g L^{-1}) and urea (0.42 M). The suspension, thermostated at 80 °C, was vigorously stirred for 4 h, until pH 8 was reached. The slurry was then centrifuged and the recovered powder was re-suspended in water and reduced by addition of a large excess of $NaBH_4$, under stirring. The suspension color turned from white to grey, indicating the reduction of Pt(IV) to metallic NPs. The so-obtained powder was repeatedly washed with water until the content of chloride ions in the supernatant was below 1 ppm and finally dried at 70 °C overnight. These materials constitute the "DP series" and were labeled as P25/Pt(x)DP, with x referring to the Pt nominal weight percent content with respect to TiO_2. For each photocatalyst series a reference sample was also prepared from P25 by following exactly the above described procedure except for the addition of the metal precursor. These samples were labelled as P25_Y (with Y = C or DP).

TiO_2 – based photocatalysts containing both Pt and Ru NPs were obtained by depositing Pt (0.8 wt.%) and Ru NPs (0.1 wt.%) by means of the DP and C methods, respectively. The so obtained materials were indicated as P25_Pt/Ru or P25_Ru/Pt, referring to the metal deposition sequence.

Taking into account the difficulties associated with ruthenium reduction in comparison to the reduction of other metals [31–33], the P25_Pt/Ru powder was further reduced at 300

°C (heating rate 10 °C min^{-1}) for 1 h in a H_2 atmosphere. The so obtained sample was labelled as P25_Pt/Ru_red.

XRF analysis, performed by using a WD-XRF PANalytical Axios Advanced spectrometer (standardless software "Omnian" PANalytical), confirmed that the actual Pt and Ru contents for P25_Pt/Ru_red sample were 0.68 and 0.07 wt.%, respectively.

Alternatively, both Pt and Ru NPs (always corresponding to 0.8 wt.% and 0.1 wt.%, respectively) were deposited on P25 TiO_2 by the C method in only one step. In this case both Pt and Ru NPs were pre-stabilized in the same colloidal suspension before their deposition on the TiO_2 surface according to the previously described procedure. The so prepared material was named P25/Pt(0.8)-Ru(0.1)C.

Finally a photocatalyst obtained by modifying P25 TiO_2 with only 0.1 wt.% of Ru NPs deposition through the C method, *i.e.* P25/Ru(0.1)C, was also investigated.

2.3. Photocatalysts characterization

X-ray powder diffraction (XRPD) patterns were recorded on a Philips PW3020 powder diffractometer using the Cu Kα radiation (λ = 1.54056 Å). Quantitative phase analysis was made by the Rietveld refinement method using the "Quanto" software. The BET specific surface area (SSA) was measured by N_2 adsorption at liquid nitrogen temperature (77 K) on a ASAP 2020 apparatus, after out-gassing in vacuo at 150 °C for at least 2 h.

HR-TEM analysis was carried out with a JEOL JEM 2010 electron microscope, equipped with a LAB6 electron gun operating at 200 keV and a Gatan CCD camera allowing high-resolution imaging. Specimens for HRTEM analysis were sonicated in 2-

propanol and then transferred as a suspension to a copper grid covered with a holey carbon film.

Diffuse reflectance (R) spectra of the photocatalyst powders were recorded on a Jasco V-670 spectrophotometer equipped with a PIN-757 integrating sphere, using barium sulphate as a reference, and then converted into absorption (A) spectra (A = 1 – R).

2.4. Photocatalytic tests

The set-up and analytical procedures adopted in this work were identical to those already used in previous studies under optimized conditions [13,15,18]. The photo-reactor consisted of a 1.1 L cylindrical Pyrex batch vessel, thermostated at 30 °C by means of an external cooling water jacket, housing an immersion UVA 25 W Jelosil HG100 mercury arc lamp emitting in the 310–400 nm wavelength range (λ_{max} ~ 365 nm). The irradiation intensity within the photo-reactor was 1.69×10^{-6} Einstein s^{-1}, according to ferrioxalate actinometry [34,35]. The TiO_2 aqueous suspensions were sonicated for 15 min, followed by NH_3 addition (initial nitrogen concentration 100 ppm, *ca.* 7 mM) and stirring in the dark for 5 min, until a stable pH was attained (always around 10–10.5). The immersion lamp was switched on at least 15 min before starting the runs and was introduced into the photo-reactor only when its emission intensity, checked by a Jelosil UVA-meter, was constant.

The irradiated suspensions contained a fixed photocatalyst amount (0.1 g L^{-1}) and were stirred at constant rate during the runs. Air was continuously bubbled in the photo-reactor at 150 mL min^{-1}. At regular time intervals, 10 mL samples of the reaction suspension were withdrawn and centrifuged. The amount of residual NH_3 (converted into non-volatile NH_4^+ salt by acidification with a H_3PO_4 aqueous solution) and of photocatalytically produced

NO_2^- and NO_3^- ions in the supernatant were determined by ion chromatography employing a Metrohm 761 Compact ion chromatograph with conductivity detection. The photocatalytic runs lasted 6 h; some photocatalysts were tested at least two times under identical conditions to check the reproducibility of the runs.

The amount of NH_3 stripped by air bubbling during the runs was evaluated by conveying the gas stream from the photo-reactor into a flask filled with 5 mM H_3PO_4 aqueous solution (ammonia trap). The concentration of NH_4^+ ions in the trap was analyzed by ion chromatography at the end of the runs and accounted for, when evaluating the amount of photocatalytically abated NH_3. Overall, the amount of NH_3 stripped during the 6 h-long runs never exceeded 2.5% of the initial NH_3 content. Moreover, previous photo-acoustic spectroscopy measurements proved that nitrogen-containing gas species such as NO, NO_2 and N_2O were not produced during the runs [15].

3. Results and discussion

3.1. Photocatalyst characterization

XRPD and BET analysis confirmed that the adopted Pt NPs deposition procedures did not affect the phase composition and surface area of P25 TiO_2 (80:20 anatase:rutile and 48 $m^2\ g^{-1}$, respectively), as already verified in previous studies [19,36].

The UV-vis absorption spectra of the DP series of Pt/TiO_2 photocatalysts together with those of P25_C and P25/Pt(0.8)C samples are collected in Fig. 1a. Reference samples of both series (containing no Ru NPs) show a slightly red-shifted absorption with respect to P25 TiO_2, probably related to a slight enlargement of the anatase crystallites, yet not detectable by XRD analysis.

Pt-modified powders show the typical broad, almost constant absorption extending over the entire visible region, which becomes progressively more intense with increasing Pt loading on TiO_2, as clearly evidenced for the DP series in similar materials [13]. Interestingly, by considering materials with a fixed nominal Pt loading of 0.8 wt.%, the spectrum of P25/Pt(0.8)C shows a distinctive profile, characterized by a linear absorption increase with increasing wavelength in the visible region, while this increase is not observed in the absorption spectrum of for P25/Pt(0.8)DP (see Fig. 1a). This suggests that the particle size distribution obtained by employing the colloidal deposition method is different from that obtained with the DP method for similar amounts of deposited Pt NPs on the TiO_2 surface.

The absence of specific *d-d* transition (in the 450-700 nm region) in the diffuse reflectance spectrum of P25/Ru(0.1)C shown in Fig. 1b confirms that effective pre-formation and stabilization of metallic Ru NPs is achieved in the colloidal suspensions after $NaBH_4$ addition, which prevents the deposition of Ru(III) species on the modified TiO_2 surface [31,32].

The addition of a low amount of Ru NPs, *i.e.* 0.1 wt.%, does not substantially modify the absorption feature of Pt-containing TiO_2, independently of the adopted sequence of the two metal co-catalysts deposition (see P25_Pt/Ru and P25_Ru/Pt in Fig. 1b) or if the C method is employed in only one step (see Fig. 2). Notably P25_Pt/Ru_red shows slightly higher absorption with respect to P25_Pt/Ru, possibly because the thermal treatment under H_2 stream promotes further reduction of both co-catalysts into metallic NPs (Fig. 1b).

The HR-TEM images shown in Fig. 3 clearly demonstrate that both the size and the distribution of Pt NPs are strongly affected by the employed deposition route. In fact, at

fixed relatively high metal loading, *i.e.* 0.8 wt.%, the DP method ensures a homogeneous and uniform immobilization of spherically shaped Pt NPs, with an average diameter of 3-5 nm (Fig. 3a), while in the case of the C series, Pt NPs clearly tend to aggregate forming nanoclusters of 3-6 units, apparently embedded between oxide particles (Fig. 3b).

The combined deposition of Pt with Ru NPs on TiO_2, followed by reduction under H_2 stream at 300 °C did not affect the original morphology and size of noble metal NPs (see Fig. 3c vs. Fig. 3a), excluding that metal particles growth and/or sintering processes occurred, at least under the here adopted thermal reduction conditions.

Interestingly P25/Pt(0.8)-Ru(0.1)C retained the unique metal NPs distribution on the TiO_2 surface attained by the C deposition method (see Fig. 3d vs. Fig. 3b).

3.2. Photocatalytic oxidation of NH_3

The effects of TiO_2 surface modification by Pt NPs immobilization were investigated, focusing on how the Pt NPs deposition technique and/or the combined deposition of Pt and Ru NPs affects the paths of ammonia photocatalytic oxidation under optimized operating conditions to attain high NH_3 conversion and selectivity towards the most innocuous intermediate oxidation product, *i.e.* N_2 [13,15].

The percent conversion of ammonia, X_{NH3} , and the selectivity S_Y toward the nitrogen-containing photo-oxidation products (Y = N_2, NO_2^- and NO_3^-) attained after 6 h-long kinetic runs carried out employing the here investigated photocatalysts were calculated from the moles of NH_3 initially contained in the suspension, $n_{NH3,i}$, the moles of NH_3, NO_2^- and NO_3^- at the end of the run, $n_{NH3,f}$, $n_{NO2^-,f}$ and $n_{NO3^-,f}$, respectively, also taking into account the amount of stripped ammonia $n_{NH3,str}$, as follows:

$$X_{NH3} = [(n_{NH3,i} - n_{NH3,f} - n_{NH3,str})/ n_{NH3,i}] \times 100 \quad (1)$$

$$S_{NO2^-} = [n_{NO2^-,f} /(n_{NH3,i} - n_{NH3,f} - n_{NH3,str})] \times 100 \quad (2)$$

$$S_{NO3^-} = [n_{NO3^-,f} /(n_{NH3,i} - n_{NH3,f} - n_{NH3,str})] \times 100 \quad (3)$$

$$S_{N2} = 100 - S_{NO2^-} - S_{NO3^-} \quad (4)$$

The selectivity to molecular nitrogen, S_{N2}, was calculated from the total nitrogen mass balance (Eq. (4)), after having ascertained that no gaseous NO_x species were produced during the runs [15]. Table 1 reports the ammonia percent conversion and selectivity results obtained by employing either the naked or the differently metal NPs modified TiO_2 photocatalysts. Of course, different selectivity values would have been obtained after different irradiation times.

The modification induced on TiO_2 by the treatment conditions adopted in each Pt deposition route had detrimental effects on the original photocatalytic activity of P25 TiO_2. In particular, P25_C was the less performing reference material in terms of percent ammonia conversion, with $X_{NH3} \approx 19\%$ *vs.* $X_{NH3} \approx 26\%$ achieved with pristine P25. This might be associated to the negative effects induced by residual amounts of chloride ions, identified on the photocatalyst surface by XPS analysis and originated from the surfactant stabilizer of Pt NPs employed in the synthesis, which may inhibit ammonia adsorption and photocatalytic oxidation.

Otherwise, all Pt-modified powders clearly exhibit an activity in ammonia conversion higher than that of naked P25 TiO_2. This effect is ascribed to a better e^-/h^+ separation induced by the ability of noble metal NPs to efficiently capture conduction band electrons [7,13], their Fermi level being lower in energy than the conduction band edge of TiO_2. This

makes valence band holes more readily available for oxidation reactions. Moreover, the photoactivity of Pt-modified TiO_2 showed a bell-shaped trend with increasing metal NPs loading, with maximum X_{NH3} for samples containing 0.3 wt.% and 0.8 wt.% for the DP and C series, respectively.

Interestingly, the ammonia photo-oxidation paths in terms of products selectivity depend on the method employed for metal NPs deposition on TiO_2, which was shown to affect also the distribution of Pt NPs, as previously evidenced by HR-TEM images (Fig. 3). In particular, while the DP method ensured the highest selectivity to NO_2^-, the colloidal C route led to the conversion of ammonia also into the other two main NO_3^- and N_2. The specific behavior of photocatalysts obtained by each deposition method can be better appreciated by considering the concentration profiles of the nitrogen-containing species as a function of irradiation time during NH_3 oxidation. Some examples are shown in Fig. 4.

For instance, P25/Pt(0.8)C and P25/Pt(0.8)DP promote a different distribution of N-containing oxidation products, though being characterized by the same nominal Pt NPs amount. In particular when P25/Pt(0.8)C was employed as photocatalyst, the concentration of nitrite ions increased up to a maximum value after ca. 3 h and then decreased, when the nitrite into nitrate ions conversion proceeded faster than NO_2^- formation from ammonia. Thus the formation of nitrate ions seems to mainly occur through two consecutive reactions [13,15], the first one consisting in the NH_3 conversion into NO_2^-, followed by NO_2^- further oxidation into nitrate ions. This resulted in a higher selectivity (> 43%) towards NO_3^- species for all photocatalysts of the C series (Table 1). In contrast, as shown for P25/Pt(0.8)DP in Fig. 4, for photocatalysts obtained through the DP method the accumulation of intermediate NO_2^- ions appears to be favoured, at least up to 6 h

irradiation, accompanied by a rather steady over time production of NO_3^- ions (Fig. 4). S_{NO2}^- was consequently higher than 54%, especially for DP materials containing relatively high amounts of noble metal NPs (0.5-0.8 wt.%).

Thus, the method employed to deposit Pt NPs on TiO_2 affects the investigated photocatalytic process more in terms of products selectivity than in relation to the percent of ammonia conversion, always ranging from 36 to 44%. Different photocatalytic paths may prevail in the presence of different distribution of Pt NPs, which can be anchored on the titania surface in the form of nanoclusters or into homogeneous spherical NPs by choosing the C or DP method, respectively.

Ru-modified P25/Ru(0.1)C was less photoactive than naked P25, but slightly more efficient than the corresponding P25_C blank sample in terms of ammonia percent conversion (Table 1). The extent of increased charge carriers separation on metal modified TiO_2 can be related to the work function value ϕ of the specific metal, *i.e.* the energy required to promote an electron from the Fermi energy level into vacuum (the higher is ϕ, the lower in energy is the Fermi level). In particular, the relatively small beneficial effect on the photocatalytic conversion of ammonia attained by Ru NPs deposition on TiO_2 may be ascribed to the quite similar ϕ values of metallic Ru and TiO_2, *i.e.* 4.71 and 4.6-4.7 eV, respectively. Consequently, the generated Schottky barrier, *i.e.* the electronic potential barrier at the metal–semiconductor heterojunction is not so high and the transfer of photoexcited electrons to Ru NPs is less efficient with respect to that towards Pt NPs, platinum being characterized by a relatively higher work function (ϕ = 5.93 eV). Though being less efficient at promoting electron-hole pairs separation, Ru NPs deposition on TiO_2 appears to limit the formation of nitrate anions and intrinsically favor NH_3 conversion into

mildly oxidized and innocuous N_2 [37]. In particular, as shown in Fig. 5, when P25/Ru(0.1)C was employed as photocatalyst, the selectivity to N_2, S_{N2}, increased during the run with a simultaneous mirroring decrease of S_{NO2^-}, suggesting nitrite ions as precursors of N_2 photocatalytic evolution. In fact, nitrite ions, formed upon the direct or indirect interaction of NH_3 with photoproduced holes on the photocatalyst surface, may further combine with ammonia molecules adsorbed on the TiO_2 surface or undergo a series of chain redox reactions, directly involving ammonia in activated form, $(NH_2)_{ox}$, also yielding N_2 [9,38–40]. This prompted us to deepen the potential role played by Ru NPs on the mechanism of ammonia oxidation attained with highly performing Pt-modified TiO_2 samples.

The combination of Pt (0.8 wt.%) and Ru (0.1 wt.%) NPs deposition on TiO_2, attained by means of DP and C methods, respectively, independently of the deposition sequence, led to both a satisfying X_{NH3} value and an increased selectivity towards NO_2^- (see P25_Pt/Ru and P25_Ru/Pt with respect to P25/Pt(0.8)DP in Table 1). Further reduction of the photocatalyst under H_2 stream at 300 °C (P25_Pt/Ru red) led to an even higher conversion of NH_3 in NO_2^- anions, with a S_{N2} value of *ca.* 70% (Table 1). This confirms the peculiar photocatalytic feature of Ru NPs in preventing, or at least retarding, nitrite into nitrate photoconversion. This greatly favors the stabilization of species containing nitrogen in intermediate oxidation states and thus more prone to disproportionate on the TiO_2 activated surface, with the final production of N_2.

The peculiar ability of Ru NPs to push ammonia decomposition selectively towards nitrite anions was proved also with the photocatalyst prepared by depositing both Pt and Ru NPs (0.8 wt.% and 0.1 wt.%, respectively) on TiO_2 through the C method in only one step,

i.e. P25/Pt(0.8)-Ru(0.1)C. As shown in Table 1, with this photocatalyst X_{NH3} decreased to 34%, while S_{NO2^-} increased to 56.6%, with S_{NO3^-} and S_{N2} both being around 22%. The concentration profiles of NH_3 and of the NO_2^- and NO_3^- ions vs. irradiation time determined in the presence of P25/Pt(0.8)C and P25/Pt(0.8)-Ru(0.1)C, shown in Fig. 4, demonstrate that the addition of small amounts of Ru NPs, though slightly lowering the NH_3 conversion rate, affects the mechanism of ammonia oxidation, enabling a higher selectivity towards nitrite ions, at the expense of NO_3^- species.

In conclusion, the peculiar selectivity obtained with Pt/Ru TiO_2-based photocatalysts can be exploited to produce almost similar concentrations of NO_2^- and NH_4^+ ions in the irradiated suspension, from which innocuous N_2 may be produced through a subsequent catalytic process under suitable conditions, which still need to be optimized [41].

4. Conclusions

Interesting effects concerning the dependence of the ammonia photodegradation mechanism on the method adopted to deposit Pt NPs on P25 TiO_2 were clearly observed. In particular, a significant formation of highly oxidized products (*i.e.* nitrate anions), was achieved in the presence of Pt NPs deposited on TiO_2 from surfactant-stabilized colloidal suspensions (C method). Otherwise the use of a modified version of the well-known deposition-precipitation (DP) route to anchor the same amount of noble metal NPs (*i.e.* 0.8 wt.%) ensured a higher stabilization towards NO_2^- ions, whose further oxidation into nitrate ions was clearly hindered, though similar percent of ammonia conversion were attained after six hours of irradiation.

In this regard it's worth to note that the different photocatalytic paths at work on the here prepared Pt/TiO_2 samples may be related to the different morphological distribution of Pt NPs, which can be deposited on the titania surface in the form of nanoclusters or into homogeneous spherical NPs by choosing the C or DP method, respectively.

Finally, though being less efficient at promoting the electron-hole pairs separation, Ru NPs deposited on TiO_2 were found to selectively push ammonia decomposition towards nitrite anions, especially if employed as co-catalyst with Pt NPs.

Acknowledgments

The collaboration of Perrucchini Sara (Istituto ENI Donegani, Novara, Italy) in XRF analysis is greatfully acknowledged. The authors M.V.D., S.B. and E.S. thank Eni S.p.A. for the financial support to this work (contract no. 3500026836). The present work received support also from the Cariplo Foundation project entitled *Novel Photocatalytic Materials Based on Heterojunctions for Solar Energy Conversion* (grant 2013-0615).

References

[1] J. Webb, H. Menzi, B.F. Pain, T.H. Misselbrook, U. Dämmgen, H. Hendrikse, H. Döhler, Environ. Pollut. 135 (2005) 399–406.

[2] M. Kaneko, G. Gokan, N. Katakura, Y. Takei, M. Hoshino, Chem. Commun. (2005) 1625–1627.

[3] H. Wang, Y. Su, H. Zhao, H. Yu, S. Chen, Y. Zhang, X. Quan, Environ. Sci. Technol. 48 (2014) 11984–11990.

[4] J. Nemoto, N. Gokan, H. Ueno, M. Kaneko, J. Photochem. Photobiol. A Chem. 185 (2007) 295–300.

[5] H. Park, Y. Park, W. Kim, W. Choi, J. Photochem. Photobiol. C Photochem. Rev. 15 (2013) 1–20.

[6] M. Duca, M.T.M. Koper, Energy Environ. Sci. (2012) 9726–9742.

[7] J. Lee, H. Park, W. Choi, Environ. Sci. Technol. 36 (2002) 5462–5468.

[8] H.H. Ou, M.R. Hoffmann, C.H. Liao, J.H. Hong, S.L. Lo, Appl. Catal. B Environ. 99 (2010) 74–80.

[9] M. Kaneko, H. Ueno, R. Saito, J. Nemoto, Catal. Letters 137 (2010) 156–162.

[10] M.V. Dozzi, G.L. Chiarello, E. Selli, J. Adv. Oxid. Technol. 13 (2010) 305–312.

[11] M.V. Dozzi, A. Saccomanni, M. Altomare, E. Selli, Photochem. Photobiol. Sci. (2012) 595–601.

[12] M.V. Dozzi, A. Saccomanni, E. Selli, J. Hazard. Mater. 211 (2012) 188–195.

[13] M. Altomare, E. Selli, Catal. Today 209 (2013) 127–133.

[14] S. Shibuya, S. Aoki, Y. Sekina, I. Mikami, Appl. Catal. B Environ. 138 (2013) 294–298.

[15] M. Altomare, G.L. Chiarello, A. Costa, M. Guarino, E. Selli, Chem. Eng. J. 191 (2012) 394–401.

[16] H. Gekko, K. Hashimoto, H. Kominami, Phys. Chem. Chem. Phys. 14 (2012) 7965.

[17] H. Kominami, H. Nishimune, Y. Ohta, Y. Arakawa, T. Inaba, Appl. Catal. B Environ. 111-112 (2012) 297–302.

[18] M. Altomare, M.V. Dozzi, G.L. Chiarello, A. Di Paola, L. Palmisano, E. Selli, Catal. Today 252 (2015) 184–189.

[19] M.V. Dozzi, L. Prati, P. Canton, E. Selli, Phys. Chem. Chem. Phys. 11 (2009) 7171–7180.

[20] R. Zanella, S. Giorgio, C.R. Henry, C. Louis, J. Phys. Chem. B 106 (2002) 7634–7642.

[21] X.M. Yang, X.N. Wang, J.S. Qiu, Appl. Catal. A 382 (2010) 131–137.

[22] Z.Y. Sun, Z.M. Liu, B.X. Han, Y. Wang, J.M. Du, Z.L. Xie, G.J. Han, Adv. Mater. 17 (2005) 928–932.

[23] W. Wang, S.P. Wang, X.P. Ma, J.L. Gong, Chem. Soc. Rev. 40 (2011) 3703–3727.

[24] Y. Zhu, S.R. Zhang, Y.C. Ye, X.Q. Zhang, L. Wang, W. Zhu, F. Cheng, F. Tao, ACS Catal. 2 (2012) 2403–2408.

[25] T. Sobczynski, A. Jakubowska, S. Zielinski, Monatsh. Chem. 120 (1989) 101–109.

[26] K. Wetchakun, N. Wetchakun, S. Phanichphant, Adv. Mater. Res. 55 (2008) 853–856.

[27] S. Kundu, A.B. Vidal, M.A. Nadeem, S.D. Senanayake, H. Idriss, P. Liu, J.A. Rodriguez, D. Stacchiola, J. Phys. Chem. C 117 (2013) 11149−11158.

[28] A.Q. Wang, C.M. Chang, C.Y. Mou, J. Phys. Chem. B 109 (2005) 18860–18867.

[29] G.L. Chiarello, M.H. Aguirre, E. Selli, J. Catal. 273 (2010) 182–190.

[30] G.L. Chiarello, A. Di Paola, L. Palmisano, E. Selli, Photochem. Photobiol. Sci. 10 (2011) 355–360.

[31] P.S.S. Kumar, A. Manivel, S. Anandan, M. Zhou, F. Grieser, M. Ashokkumar, Colloids Surfaces A Physicochem. Eng. Asp. 356 (2010) 140–144.

[32] K. Vinodgopal, Y. He, M. Ashokkumar, F. Grieser, J. Phys. Chem. B 110 (2006) 3849–52.

[33] C. Li, S. Zhang, B. Zhang, D. Su, S. He, Y. Zhao, J. Liu, F. Wang, M. Wei, D.G. Evans, X. Duan, J. Mater. Chem. A 1 (2013) 2461.

[34] C.G. Hatchard, C.A. Parker, Proc. R. Soc. London, Ser. A 235 (1956) 518–536.

[35] M. Mrowetz, E. Selli, New J. Chem. 30 (2006) 108–114.

[36] M. Mrowetz, A. Villa, L. Prati, E. Selli, Gold Bullettin 40 (2007) 154–160.

[37] M.V. Dozzi, E. Selli, J. Adv. Oxid. Technol. (2016) accepted.

[38] S. Yamazoe, T. Okumura, Y. Hitomi, T. Shishido, T. Tanaka, J. Phys. Chem. C 111

(2007) 11077–11085.

[39] S. Yamazoe, T. Okumura, T. Tanaka, Catal. Today 120 (2007) 220–225.

[40] H. Yuzawa, T. Mori, H. Itoh, H. Yoshida, J. Phys. Chem. C 116 (2012) 4126–4136.

[41] D.K. Lee, S.C. Jeong, L.Y. Wang, Chemosphere 61 (2005) 573–578.

Table 1

Ammonia conversion (X_{NH3}) and product selectivity of naked and metal modified TiO_2 photocatalysts.

Sample	X_{NH3} (%)	Selectivity (%)		
		NO_2^-	NO_3^-	N_2
P25	25.7	31.2	26.9	41.9
P25_DP	21.7	35.9	16.9	47.2
P25_C	18.9	33.2	19.3	47.5
P25/Ru(0.1)C	23.4	32.6	18.8	48.6
P25/Pt(0.3)DP	42.6	26.3	40.5	33.2
P25/Pt(0.5)DP	39.1	54.2	27.1	18.7
P25/Pt(0.8)DP	40.5	57.0	22.4	20.6
P25/Pt(0.3)C	35.6	12.7	43.3	44.0
P25/Pt(0.5)C	41.3	11.9	47.4	40.7
P25/Pt(0.8)C	43.8	14.9	47.7	37.4
P25_Ru/Pt	36.1	65.8	16.8	17.4
P25_Pt/Ru	39.3	60.2	19.9	19.9
P25_Pt/Ru_red	38.7	70.6	19.0	10.4
P25/Pt(0.8)-Ru(0.1)C	34.0	56.6	21.4	22.0

Figure captions

Fig. 1. Absorption spectra of (a) Pt-modified P25 TiO_2 and of (b) Pt- and Ru-modified P25 TiO_2. Absorption spectra of unmodified P25 and of P25_C and P25_DP reference materials are also included for comparison.

Fig. 2. Absorption spectra of P25 TiO_2 modified by only Pt NPs or by Pt and Ru NPs deposition through the colloidal (C) method.

Fig. 3. HR-TEM images of (a) P25/Pt(0.8)DP, (b) P25/Pt(0.8)C, (c) P25_Pt/Ru_red and (d) P25/Pt(0.8)-Ru(0.1)C.

Fig. 4. Concentration profiles of NH_3, NO_2^- and NO_3^- during ammonia photocatalytic oxidation on Pt and/or Ru NPs-modified photocatalysts.

Fig. 5. Ammonia conversion X_{NH_3} and selectivity to N_2, NO_2^- and NO_3^- during the run carried out with P25/Ru(0.1)C.

Fig. 1.

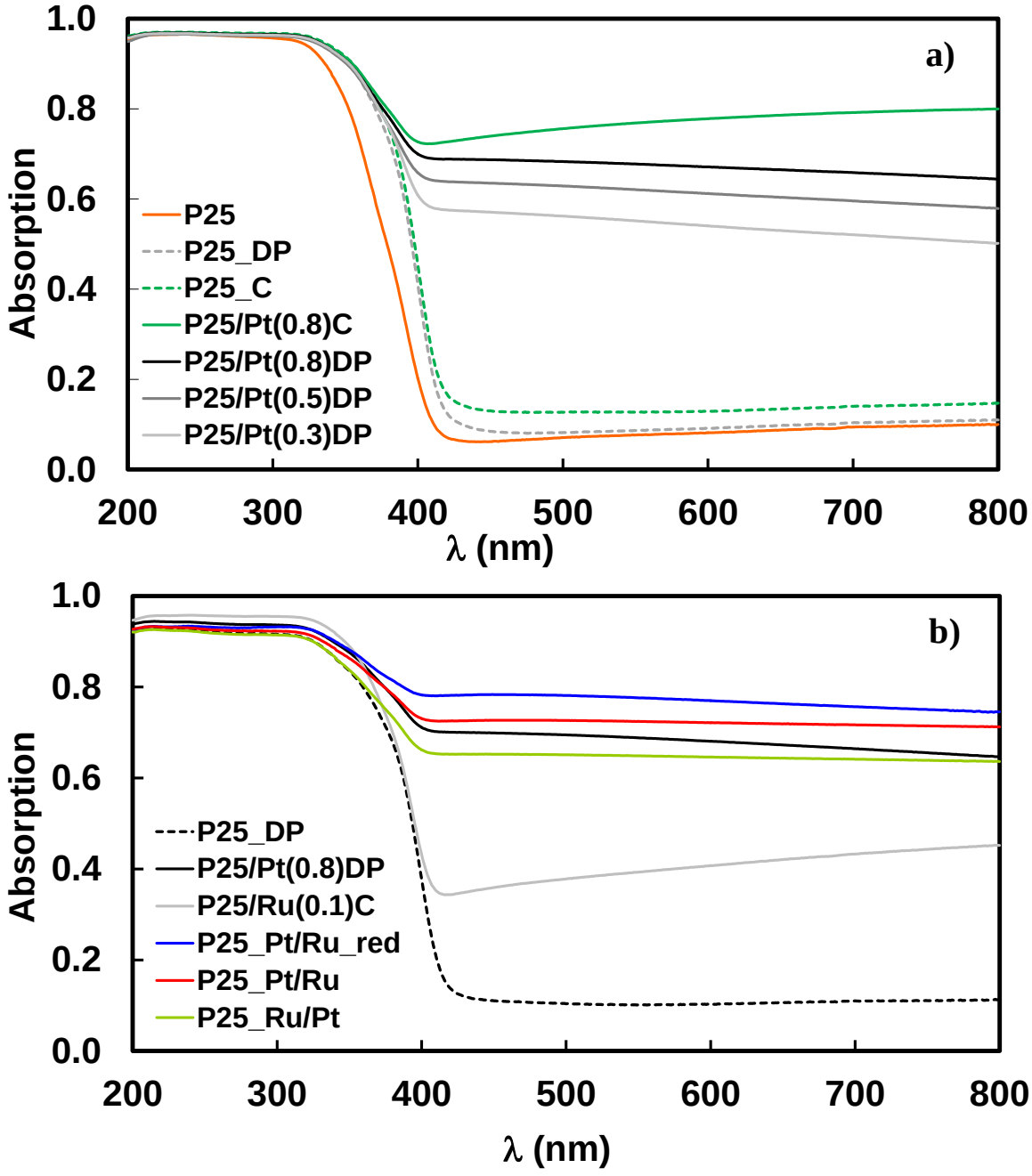
a)
Absorption
λ (nm)
P25
P25_DP
P25_C
P25/Pt(0.8)C
P25/Pt(0.8)DP
P25/Pt(0.5)DP
P25/Pt(0.3)DP
b)
Absorption
λ (nm)
P25_DP
P25/Pt(0.8)DP
P25/Ru(0.1)C
P25_Pt/Ru_red
P25_Pt/Ru
P25_Ru/Pt

Fig. 2.

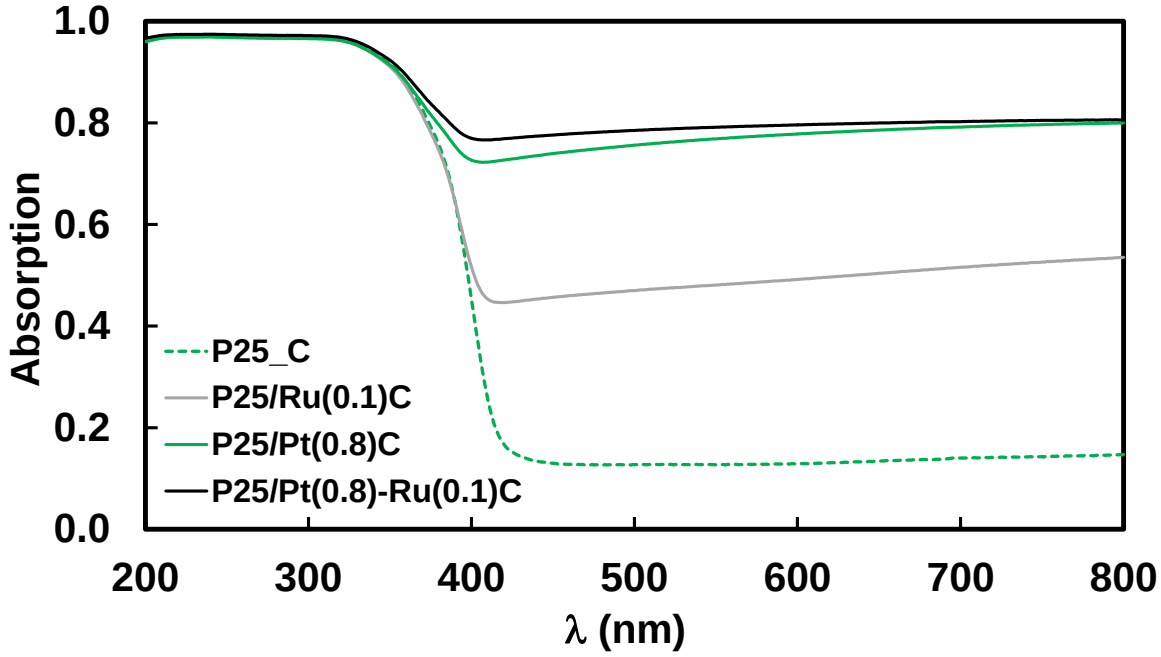
1.0
0.8
0.6
0.4
0.2
0.0
Absorption
P25_C
P25/Ru(0.1)C
P25/Pt(0.8)C
P25/Pt(0.8)-Ru(0.1)C
200
300
400
500
600
700
800
λ (nm)

Fig. 3.

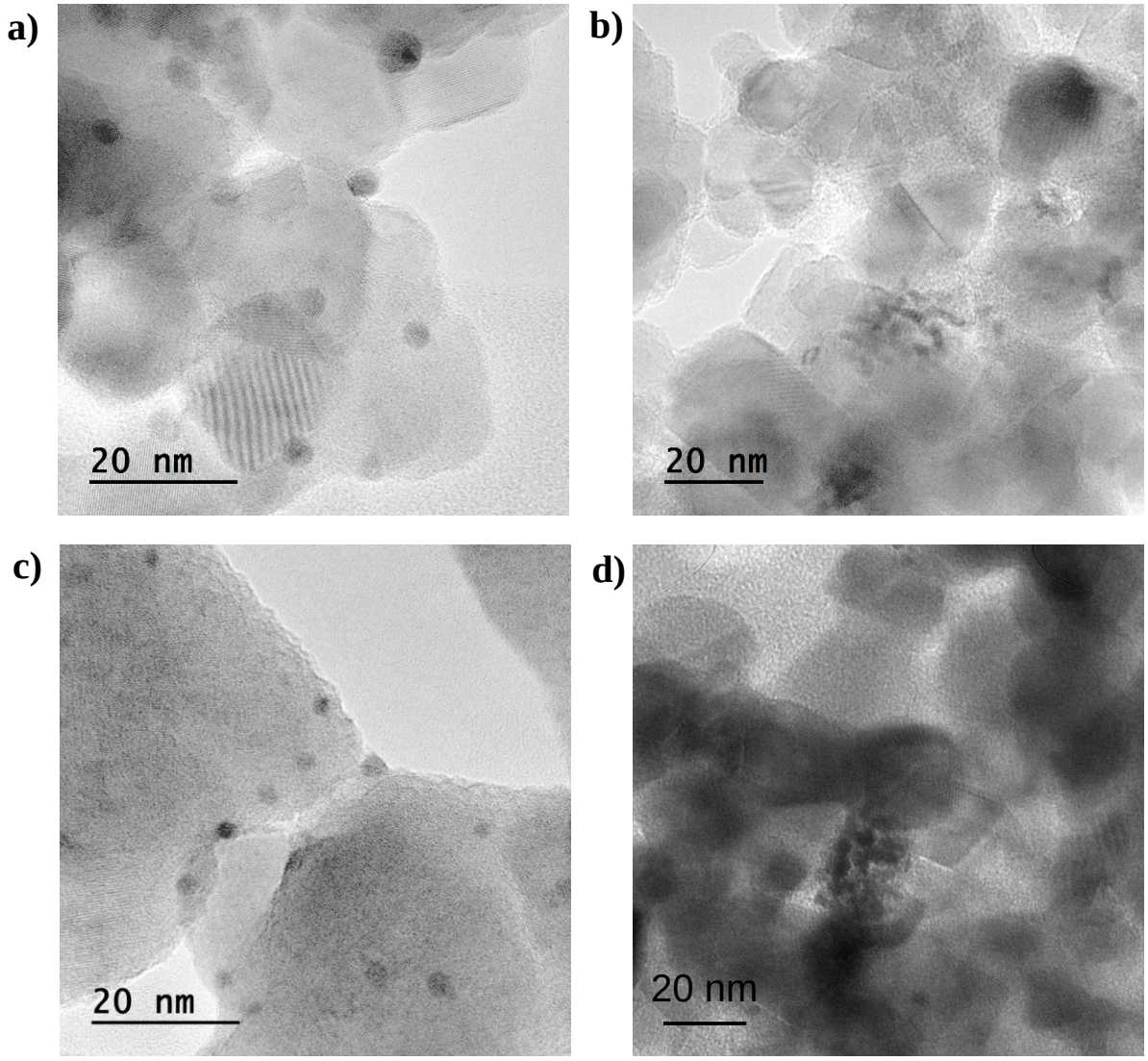

Fig. 4.

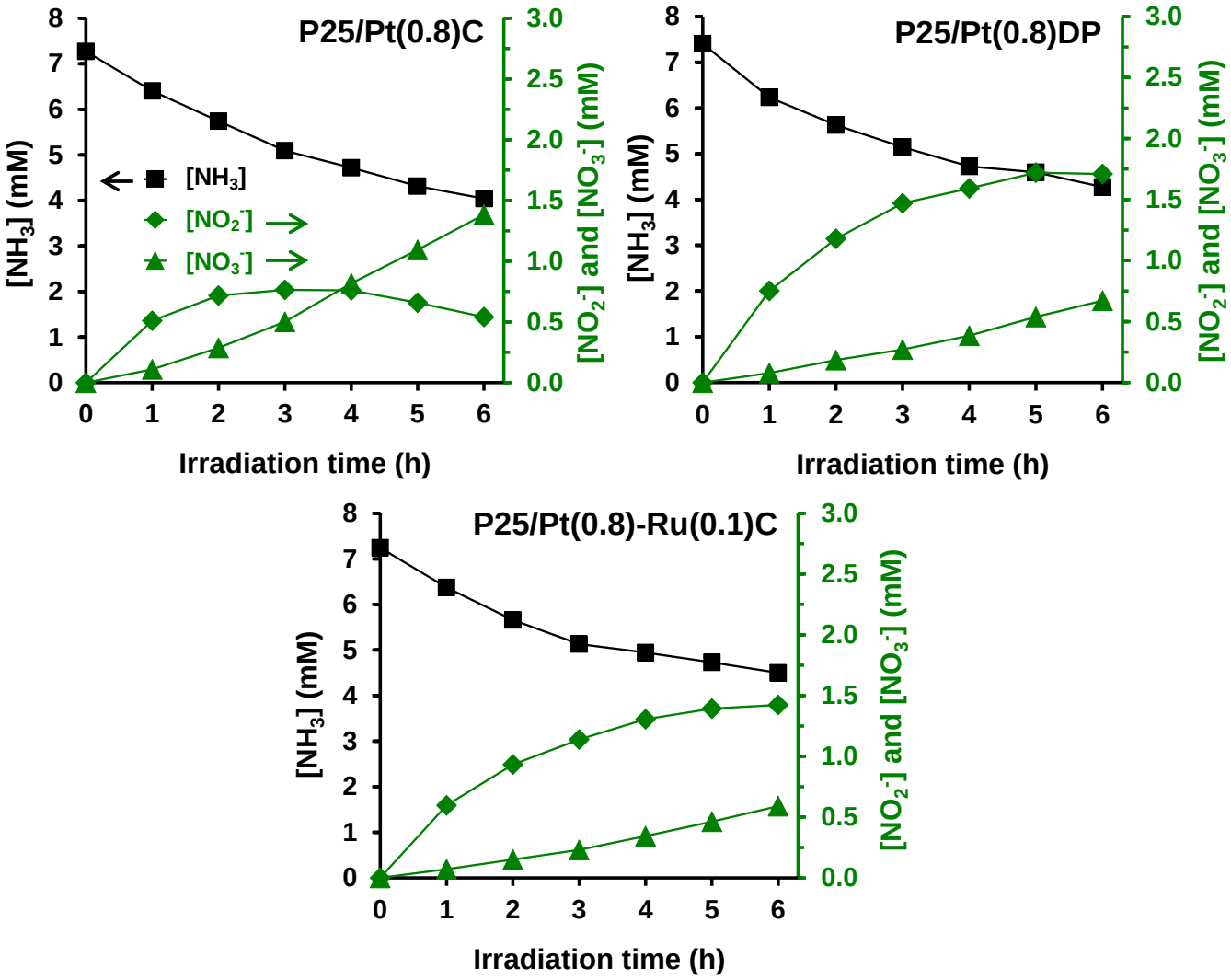
P25/Pt(0.8)C
P25/Pt(0.8)DP
P25/Pt(0.8)-Ru(0.1)C
[NH3] (mM)
[NO2-] and [NO3-] (mM)
Irradiation time (h)
[NH3]
[NO2-]
[NO3-]

Fig. 5.

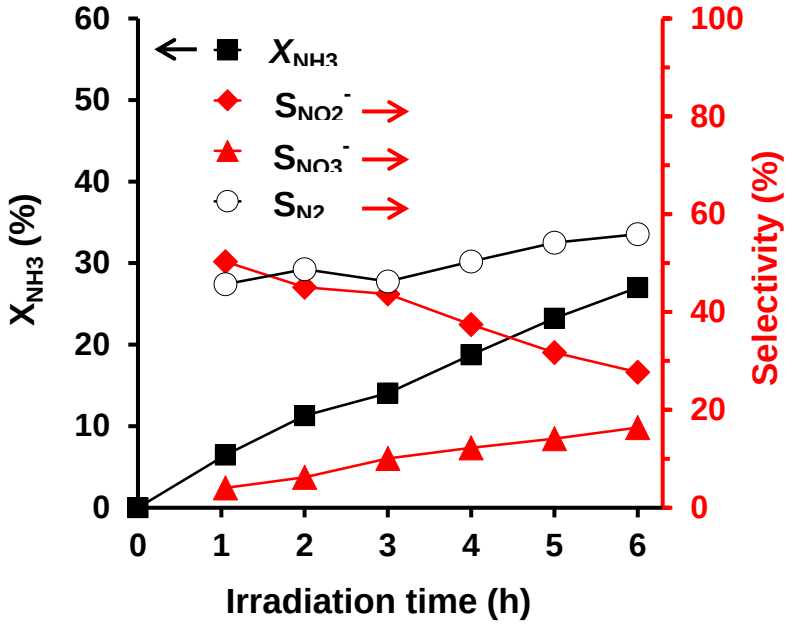
60
50
40
30
20
10
0
X_{NH3} (%)
100
80
60
40
20
0
Selectivity (%)
X_{NH3}
S_{NO2}^-
S_{NO3}^-
S_{N2}
0
1
2
3
4
5
6
Irradiation time (h)